Geomechanics and Engineering, *Vol. 34, No. 6 (2023) 665-681*
https://doi.org/10.12989/gae.2023.34.6.665

Investigating the dynamic response of deep soil mixing and gravel drain columns in the liquefiable layer with different thickness

Gholi Asadzadeh Khoshemehr and Hadi Bahadori*

Department of Civil Engineering, Urmia University, Urmia, Iran

(*Received February 20, 2022, Revised August 15, 2022, Accepted August 16, 2022*)

Abstract. Liquefaction is one of the most devastating geotechnical phenomena that severely damage vital structures and lifelines. Before constructing structures on problematic ground, it is necessary to improve the site and solve the geotechnical problem. Among ground improvement methods dealing with liquefaction, gravel drain (GD) columns and deep soil mixing (DSM) columns are popular. In this study, the results of a series of seismic experiments in a 1g environment on a structure located over liquefiable ground with different thicknesses reinforced with GD and DSM techniques were presented. The dynamic response of the reinforced ground system was investigated based on the parameters of subsidence rate, excess pore water pressure ratio, and maximum acceleration. The time history of the input acceleration was applied harmonically with an acceleration range of 0.2g and at frequencies of 1, 2, and 3 Hz. The results show that the thickness of the liquefiable layer and the frequency of the input motion have a significant impact on the effectiveness of the improvement method and all responses. Among the two techniques used, DSM in thick liquefied layers was much more efficient than GD in controlling the subsidence and rupture of the soil under the foundation. Maximum settlement values, settlement rate, and foundation rotation in the thicker liquefied layer at the 1-Hz input frequency were higher than at other frequencies. At low thicknesses, the dynamic behavior of the GD was closer to that of the DSM.

Keywords: deep soil mixing; gravel drain; liquefaction; settlement; shaking table; soil improvement

1. Introduction

Liquefaction-induced ground deformation is one of the major seismic hazards that cause damage to buildings, infrastructure, roads, bridges, and even loss of human life, as reported in previous seismic events (Cubrinovski *et al.* 2011). Earthquakes in liquefiable areas are typically followed by settlement of surface structures. In the great earthquake of 2011 in eastern Japan, massive liquefaction damage occurred in the coastal areas of Tokyo Bay and in the Tone River basin. The subsidence and overturning of residential buildings was more than 27,000 buildings (Miyajima *et al.* 2019). October 2011 Van earthquake of Turkey which was felt in Urmia University (the place of this research), caused a lot of damage to buildings and lifelines (Ozden *et al.* 2014). Kayabasi and Gokceoglu (2018) conducted a series of studies to evaluate the liquefaction potential of Eskişehir, Turkey. Liu and Dobry (1997) carried out eight centrifuge tests to investigate settlement features of circular foundations situated on liquefiable soils. The result of their study indicated that settlement percentage is dependent upon the width of the foundation and thickness of liquefiable layer.

Therefore, the liquifiable layer thickness is one of the governing factors in the adopted countermeasure technics. When choosing land reclamation methods to deal with liquefaction, factors such as effectiveness, reliability, cost-effectiveness, time, construction conditions, soil type, and environmental compatibility should be considered (Porbaha *et al.* 1999, Shahraki *et al.* 2018). Among the soil improvement methods, deep soil mixing (DSM) columns and gravel drain (GD) columns can be highlighted, especially in urban areas. These techniques have a short construction time and low cost. They also have much less vibration and noise pollution than compacting methods (Siddharthan and Porbaha 2008a, b). GD method is used from about 45 years ago when Seed and Booker (1977) proposed the design charts. This method has been carried out in hundreds of projects till now and is an economic method in soil treatment especially in shallow depths. On the other hand DSM method was first used in 1971 near Handa Airport in Japan. The first DSM project in the United States was carried out in 1986 under a dam on Lake Jackson and because of popularity of the method in this country, the FHWA in 1997 developed regulations (FHWA-RD-99-138) and criteria for executing the DSM method. Too many projecects have adopted DSM method to improve their problematic sites all over the world containing our country (Iran), especially in ports and marine structures. Based on the mentioned facts, the GD and DSM methods are completely adoptable in real-life which reflects that their cost-benefit ratio is acceptable especially in liquefaction cases. DSM is utilized to reduce shear strain, stress, and excess pore water pressure, and GD is used to increase drainage, shear reinforcement, and soil compaction during installation. In general, the main advantages of columnar reinforcement systems are increased bearing capacity,

*Corresponding author, Professor
E-mail: h.bahadori@urmia.ac.ir

ISSN: 2005-307X (Print), 2092-6219 (Online)

reduced settlement, reduced shear strain, and the prevention of the transfer of overpressures to other parts of the soil to counteract liquefaction. DSM columns are often used under the foundation of tall buildings with different penetration depths. The rupture mechanism and bearing capacity in soft soils reinforced with these columns are complex in the presence of overhead (Zhou *et al.* 2018). DSM is one of the most effective methods for improving liquefiable soil (Hasheminezhad and Bahadori 2019, 2020, Yang *et al.* 2021). Liquid layer thickness, input movement level, overhead pressure, foundation size effect, and the height-to-width ratio of a structure can affect the dynamic response of the improvement technique (Bertalot *et al.* 2013). Porbaha *et al*. (1999) conducted studies on DSM using a shaking table. They concluded that the combination of DSM and drainage can treat and strengthen structures. Esmaeili *et al*. (2014) investigated the effectiveness of DSM in loose sandy soils using laboratory experiments. The results show that the effectiveness of DSM depends on various parameters such as sand density and the water-to-cement ratio of mortar. In addition, DSM significantly increases the internal friction angle and soil adhesion. During the 1995 Kobe earthquake, DSM walls were found to be effective against liquefaction (Namikawa *et al.* 2007). Asgari *et al*. (2013) and Green *et al.* (2008) studied the performance of DSM using physical models. The results of centrifuge experiments showed that wall distances, wall depth, and the frequency of input movement are effective parameters in the shear performance of DSM columns, as they influence overcurrent overpressure. Tang *et al*. (2015) evaluated the impact of GD on the reduction of lateral soil displacement induced by liquefaction using numerical simulations. Bahmanpour *et al*. (2019) studied the effect of DSM columns to counteract liquefaction using a shaking table while considering several parameters such as input motion frequency, distance, the length and diameter of columns, and boundary conditions. They observed that the most important parameter affecting the performance of the columns is the flexural rigidity of the column. Also, the constraint effect of the columns to decrease the shear deformation accumulation in the soil is cited as the main effect of using columns as a countermeasure against liquefaction. Therefore, it is necessary to evaluate the response and deformation of reinforced soil against strong movements for critical structures in order to choose the most appropriate improvement method.

However, almost few comprehensive studies have been performed on the effect of different liquefaction layer thickness on the seismic performance of DSM and GD columns so far. In order to fully understand the performance of columns in the form of efficiency, performance and economic justification, it is necessary to study the dynamic behavior of columns at different thicknesses of liquid-prone sand layer. The shaking table test is an acceptable approach for learning about the dynamic performance of reinforced ground due to the inadequacy of in situ data (Zeng and Schofield 1996). In this study, a shaking table model test with a flexible box was used to analyze the seismic responses of free-field, GD and DSM columns containing soil layers. Models were implied harmonic loads with different frequency domains. The effects of the DSM and GD columns on the nonlinear dynamic response of different thicknesses of the liquefaction-prone sand layer were investigated by using parameters such as acceleration response, settlement, excess pore water pressure ratio and dynamic response of the whole system. Furthermore, the rupture of the columns in a similar area replacement ratio (A_r) is focused.

2. Model preparation

Fig. 1 shows the box in plan. Both improvement techniques were placed in one model to simultaneously evaluate the effectiveness of the improvement methods in the same conditions. It is noteworthy that the two foundations were placed at a suitable distance from one another to eliminate the effects of interaction. According to Lou *et al.* (2011), if the distance between two similar structures is more than 2.5 times the width of the foundation, the interaction effects can be neglected, and if the distance between two structures is less than the width of the foundation, the response of the structure due to interaction is about a 10% increase or decrease. In engineering projects, the diameter of GD and DSM columns is usually designed and executed between 0.5 to 1.50 meters. Furthermore, based on the site and the subsurface layers, the length-to-diameter ratio is 6 to 20. The area replacement ratio is applied between 5% and 30%, which primarily depends on the layer thickness and the degree of relative density (Yang *et al.* 2021). The geometry of the GD and DSM columns is similar in the model. In the prepared model, the arrangement of the columns is triangular, there are eight of them on each side, and their diameter is 5 cm.

The area replacement ratio (A_r) is equal to 18.2% as calculated in Fig. 2. The dimensions of the foundations are 22 cm in width, 30 cm in length, and 6 cm in thickness, with a weight of 30 kg. The material of the foundation is cast iron alloy and its specifications are the same in all tests. The foundation used represents a building of about 10 floors with a stress of 90.91 kPa beneath the foundation. The model consists of two layers: a layer of dense sandy soil at the bottom and a layer of loose sand at the top.

The modeling of DSM columns in the laboratory has been studied by various researchers. Bahmanpour *et al.* (2019) conducted a series of experiments on DSM columns' ability to reduce liquefaction hazards. They modeled DSM columns with PVC pipes with an outer diameter of 5 cm, a thickness of 2 mm, and a height of 1 m. They filled the inside of the pipes with dry sand to make them heavy enough to withstand liquefied sand-induced uplift force. Kitazume (1996) and Kitazume *et al*. (2000) performed a series of experiments using a centrifuge device to model the breakwater on DSM columns with a modified surface ratio of 79%. The diameter of these columns was 20 mm, and their length was 250 mm. The columns were modeled with PVC pipe with an inner diameter of 20 mm. Bouassida and Porbaha (2004) conducted a series of shaking table tests on DSM columns with a modified land bearing capacity. The area replacement ratio was equal to 18.8% for columns of

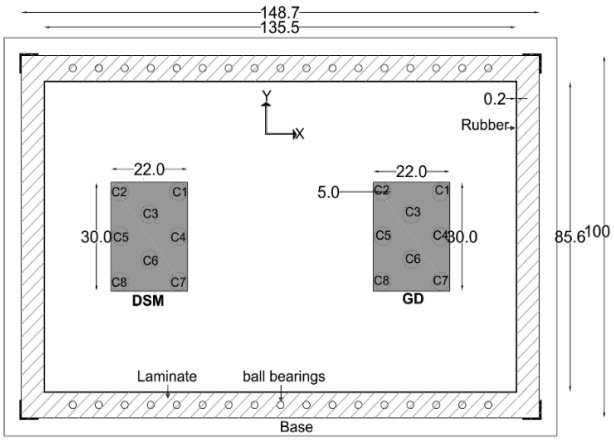

Fig. 1 Model plan (dimensions in centimeters)

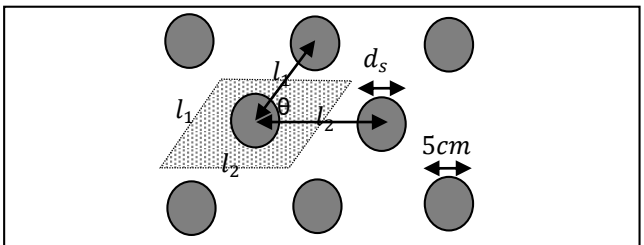

L2=22-5=17cm

L1=10.72cm

θ=36.2

$$A_r = 100 * \frac{\pi d_s^2}{4} \frac{1}{l_1 . l_2 . \sin\theta} = 18.2\%$$

Fig. 2 Calculation of area replacement ratio (Ar) in triangular pattern

different lengths. The diameter of the columns was 20 mm, and they were created by the pipe.

In the present study, the construction of columns in the sand was not feasible without special arrangements. Thus, for this purpose, PVC pipes with an outer diameter of 5 cm were used in compliance with the simulation rules. The pipes were first placed on the hard soil layer by a template and fixed. Then, the loose soil profile was created with a certain density. This method simulates the process of long auger drilling to install columns without compacting the soil in situ. A wet tamping technique was adopted to prepare the soil model, following Fattah *et al*. (2017). In this modeling process, the specific gravity of the dense layer and loose layer is 1700 kg/m3 and 1527 kg/m3 with 5% moisture, respectively. Sampling and sand cone tests were performed to control the relative density of sand layers. After the soil profile was created to produce DSM and GD columns, the pipes were taken out of the soil one by one. Then the cavities created by specific materials were filled. The mortar filling operation in the cavities in each DSM was performed in five stages. Each layer was compressed with the same number of strokes with the compression lever. The amount of uniaxial resistance and three-day modulus of elasticity in the saturated DSM column created by this method were 350 kPa and 25.5 MPa, respectively. The density of the GD column was equal to 1650 kg/m3. The amount of material, the number of vibrations, and the height of the fall in both types of columns were determined by trial

(a) Sand cone test

(b) Uniaxial test (c) Wet sand sampling

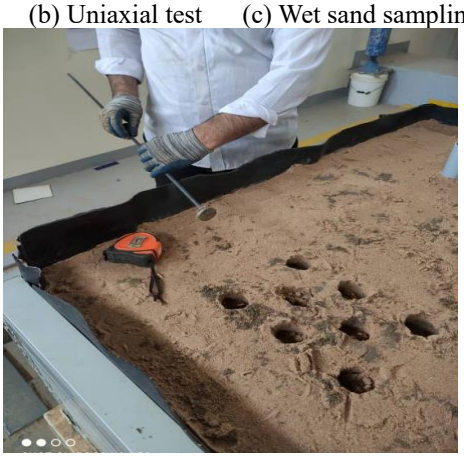

(d) Preparing a DSM column

(e) GD column

Fig. 3 DSM and GD columns implementation process

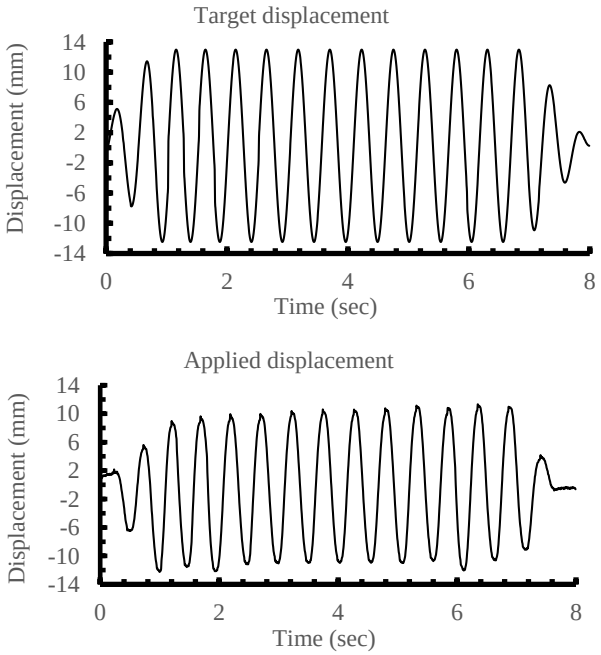

Fig. 4 A typical target and applied displacement time history of shaking table (test D5F2)

and error to achieve these goals. During compaction, the soil around the cavity should not be compacted. Fig. 3 shows the process of DSM and GD column execution.

The model is saturated before applying the harmonic load. For this purpose water flowed with a very low flow rate from the bottom level, and gradually the soil model started to become saturated. After the water level was visible on the soil surface, the saturation process was completed. It should be remembered that in order to achieve full saturation of the soil model, carbon dioxide gas was passed through the soil model before the start of the water flow process. By controlling the amount of settlement on the surface of the soil mass during the saturation process, changes in relative density were cotrolled. The variation of relative density of soil mass while saturation was negligible.

3. Section title: Level 1

3.1 Shaking table

A shaking table model with table deck dimensions of 3*2 meters and a maximum loading capacity of five tons is located in the Center for Crisis Management and Infrastructure Engineering of Urmia University. This shaking table could work with a maximum acceleration of 1.5 g, a maximum frequency of 18 Hz, and a maximum displacement of 240 mm. This device has two drive motors, each of which can reach a speed of 150 mm per second (Fig. 5).

It should be noted that seismic loading is controlled by displacement. In our experiments, a harmonic acceleration time history was implied in the models. A target displacement time history was built considering desired maximum acceleration, frequency and time of loading.

Fig. 5 A view of shaking table and laminar shear box

Based on the measured displacement on the dynamic actuator, the control software guides the applied loading utilizing a PID control system. Fig. 4 is an example of target and applied displacement time histories at a frequency of 2 Hz. The input acceleration time history was measured based on the mentioned displacement control system.

4. Laminar shear box

A flexible tank on the shaking table was designed for testing. The model tank was a rectangular laminar shear box with internal dimensions of 135.5 cm in length, 85.6 cm in width, and 72 cm in height. This tank was made of 18 single laminates supported by each other and made of aluminum profile pieces. The cross-section of the laminates was rectangular, with dimensions of 40 mm by 66 mm. The laminates were stacked one on top of the other and separated by ball bearings. The mass of each laminate was equal to 1.7 kg. Considering the relative density of the loose layer (Dr = 25%) and the dense layer (Dr = 80%), the ratio of the relative mass of a single laminate to the containing sand was 10.1% for the loose layer and 9.1% for the dense sand. Because the mass of the sand was much higher than the mass of the tank wall, the effect of the inertial force of the tank in the experiment was negligible (Prasad *et al*. 2004, Yang *et al.* 2021). A rubber layer on the inside of the box sealed the box and protected the bearings. The thickness of this layer was 2 mm, which gave it good flexibility. The basic design of the box was intended to minimize the lateral rigidity of the box because of the dominance of the soil in the response of the box-soil system. Due to the flexibility of the laminar shear box boundaries, the absorption of seismic waves occurred at the boundaries, and, as a result, the wave reflection and return to the model were almost negligible (Araei and Towhata, 2014). The bottom laminate of the box was fixed to the shaking table. The flexible box was free to move only along

Table 1 Characteristics of Firoozkuh sand No. 161 and the utilized gravel

Material	Gs	e_{max}	e_{min}	D_{50} (mm)	F_C(%)	C_u	C_c	K(cm/s)
Firoozkuh sand	2.65	0.874	0.548	0.27	1	1.87	0.88	0.0125
Gravel	2.66	.....	.....	8.5	1	2.74	0.91	7.31

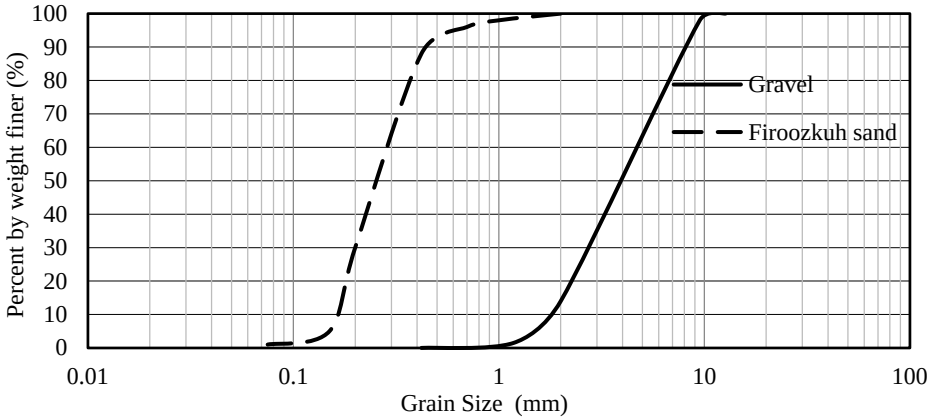

Fig. 6 Water content changes with time (evaporation rate) for treated and untreated samples

one direction and along the horizontal plane. Lee *et al.* (2012) and Turan *et al*. (2009) investigated the design and performance of the laminar shear box and the boundary effects on the seismic responses obtained from the acceleration and pore water pressure transducers based on centrifuge experiments. The results of their studies showed that if the transducers are located at a distance of more than one-twentieth of the model length from the end of the wall, then the boundary effects of the box on the maximum amplitude of acceleration, fundamental frequency, acceleration time delay, and acceleration magnification factor will be negligible.

5. Material

5.1 soil

Firoozkuh Sand No. 161, which is a clean and uniform sand, has been used in this study, the specifications of which are given in Table 1 and Fig. 6. According to the Soil Classification System (USCS), this sand is in the category of poorly graded sand (SP) (Bahadori *et al*. 2008, Farahmand *et al*. 2016).

5.2 Gravel drain (GD) columns

The particle size distribution for gravel drains is illustrated in Fig. 6. The mechanical characteristics of the gravel can be found in Table 1. In coarse materials, increasing the particle size leads to increases in permeability. However, the empty space between the particles also increases, and, as a result, the capacity for clogging increases. Therefore, the empty spaces are filled with ambient soil, and the permeability of gravel columns is reduced. Studies by Seed and Booker (1977) have shown that the permeability of gravel columns must be at least 200 times greater than the permeability of the surrounding soil to control the clogging and the quality index of gravelly materials. The state in which the drains act as an empty well is used as the basis for selecting the drain, mathematically expressed by Eq. (1).

$$\mathrm{K_d} > \mathrm{K_s}(\frac{h}{a})^2 \tag{1}$$

where Kd and Ks are coefficients of the permeability of drain and sand material respectively (in cm/s) and h and a are the drain depth and the drain radius, respectively. In order to control the clogging and the quality index of gravelly materials, it is necessary to satisfy Eq. (2).

$$\frac{D_{G15}}{\mathrm{D_{S85}}} < 5 \tag{2}$$

Where D_{G15} is the particle diameter of drainage materials finer than 15% and $\mathrm{D_{S85}}$ is the diameter of soil particles finer than 85%. The value of this ratio is equal to 4.87, which is within the allowable range. Also, if the quality index of drainage materials (SN) is less than 10, the degree of suitability of drainage materials will be excellent. This index can be expressed by Eq. (3) (Bayati and Bagheripour 2019, Brown 1977, Orense *et al*. 2003).

$$S_N = 1.7\sqrt{(\frac{3}{(D_{50})^2}+\frac{1}{(D_{20})^2}+\frac{1}{(D_{10})^2})} \tag{3}$$

Where D50, D20 and D10 are the grain diameters of which 50%, 20% and 10% of the sample grains are finer than them, respectively. In this model, the quality index is equal to 1.43. As can be seen the gravel materials used in the gravel columns provide non-clogging conditions, quality marks, and permeability. The graphs provided by Seed and Booker were used to calculate the drainage capacity of GD. In these diagrams, the characteristics of

liquefiable soil, production and excess pressure ratio of pore water, as well as the properties of liquefied soil consolidation and earthquake loading, are assumed. In the design of the columns, it is common to consider a maximum excess pore water pressure ratio (ru_{max}) of 0.25-0.5 (Brennan and Madabhushi 2002, Iai 1986).

5.3 Deep soil mixing (DSM) columns

The materials used to build DSM columns include ambient soil (Firoozkuh sand#161) and Portland cement type II, which have been created in situ with a water-to-cement ratio of unity and cement content of 110 kg/m3. Esmaeili *et al*. (2014) conducted a series of laboratory studies to investigate the effectiveness of DSM column in stabilizing loose sandy soil. The results of their research showed that the best ratio of water to cement is unity. In determining the mechanical characteristics of DSM columns in a laboratory model, first, the average shear modulus (G_{avg}) of the ambient soil mass and DSM column in the laboratory model is obtained. Then, based on the area replacement ratio (A_r), the amount of shear modulus and DSM column modulus of elasticity are obtained. In this research, different ratios in the mix design were investigated. Considering the execution method and the amount of uniaxial resistance of DSM column (between 2000 and 5000 kPa), modulus of elasticity, and curing period while applying scale laws, the percentages of the final mix design in accordance with DSM column mechanical specifications were obtained.

The mechanical specifications of the DSM column prototype include Diameter (D_{dsm}=1 m), area replacement ratio (A_r=18.2%), modulus of elasticity (E_{dsm}=100 MPa), shear modulus (G_{dsm}=42 MPa), and uniaxial resistance (qu=3.5 MPa).

6. Scale law

Although it is impossible to estimate all the simulation requirements in 1g experiments, a number of important factors influencing the experiments can be considered. One of the most important parameters is the improved ground shear modulus (Gavg), which plays an important role in the effect of the group of underground columns on liquefaction and foundation subsidence. The reason might be related to the effect of columns on maintaining the stiffness of the surrounding soil. In this study, the simulation relationships extracted by Iai (1989) were utilized. According to the engineering projects and the dimensions of the box, the geometric scale was set to 20. Estimated increases in the shear strength of soil due to DSM columns can be determined by different methods. One method is based on shear strain compatibility between columns and ambient soil, and another method assumes that there is a shear strain difference between DSM columns and ambient soil. These analytical methods can be used to obtain a moderate shear modulus for modified soils. Shear strain incompatibility increases when the stiffness of the columns relative to the surrounding soil is increased. According to Rayamajhi *et al.* (2014), the ratio of the average shear modulus for modified soil (G_{avg}) to the shear modulus at low strain for unmodified soil (G_s) can be estimated by Eqs. (4) and (5).

Table 2 Scale relationships between model and prototype

Parameters	Scale factors (Prototype/model)	Prototype	Model
Geometry	N(equal to 20)	1.00	0.05
Pile Diameter (cm)	N	100.00	5.00
Density of soil (kN/m^3)	1	15.27	15.27
Foundation stress (kPa)	N	90.91	4.55
Acceleration	1	0.20 g	0.20 g
porosity of soil (%)	1	0.44	0.44
Average shear modulus (Mpa)	$(N)^{0.5}$	10.1	2.24

$$\frac{G_{\mathrm{avg}}}{\mathrm{G_s}} = \left(\frac{\tau_{avg}}{\gamma_{avg}}\right).\frac{1}{G_s} = \frac{1 + A_r.(\gamma_r.G_r - 1)}{1 + A_r.(\gamma_r - 1)} \tag{4}$$

$$\gamma_r = \frac{\gamma_{soil-cement}}{\gamma_{\mathrm{soil}}} = 1.04(\mathrm{G_r})^{-0.65} - 0.04$$
$$\mathrm{G_r} = \frac{G_c}{G_s} \tag{5}$$

In which τ_{avg} and γ_{avg} are the average shear stress and shear strain in the soil, respectively, and G_c is column shear modulus at low strain. Meanwhile, γ_r is the shear strain ratio, $\gamma_{soil\text{-}cement}$ is the shear strain in the cement-soil column, A_r is the area replacement ratio of the columns, and γ_{soil} is the shear strain in the soil. These formulas consider the shear strain incompatibility conditions between the columns and the surrounding soil using the γ_r parameter. When the value of γ_r is equal to unity, these equations consider the shear strain compatibility conditions between the surrounding soil and the columns (DehqanKhalili *et al.* 2020). In this case, the average shear modulus value will be $G_{avg} = G_s.(1\text{-}A_r) + G_c.A_r$. Due to the lack of large stiffness differences between the columns and the soil, shear strain compatibility conditions were considered in the calculations. The scale relationships and results are presented in Table 2.

7. Monitoring tools

Fig. 7 shows the location of the transducers in the model. Nine acceleration, four pore water pressure, and three displacement transducers were utilized. Acceleration transducers were placed at three heights of 25, 45, and 60 cm from the base. One acceleration transducer was located on the table to record the input, and two acceleration transducers were placed on the foundations. Four pore water pressure sensors were located at two heights of 35 and 52.5 cm from the bottom of the box. The subsidence of the foundations was controlled by LVDT transducers located at the center of the foundation surface.

As shown in Fig. 7, the foundations are placed on a gravel blanket with a thickness of 2.5 cm on the top of

Table 3 Details of performed tests

Test series	Test NO.:	Number of tests	DSM & GD		Loading frequency (Hz)	Thickness of layers (cm)	
			Diameter (cm)	Length (cm)		h2 (cm)	h2 (cm)
1	A	…	No	No	2	65	5
2	D5F1			65	1	65	5
3	D5F2	D5	5	65	2	65	5
4	D5F3			65	3	65	5
5	D30F1			40	1	40	30
6	D30F2	D30	5	40	2	40	30
7	D30F3			40	3	40	30
8	D50F1			20	1	20	50
9	D50F2	D50	5	20	2	20	50
10	D50F3			20	3	20	50

The relative density of the loose layer is equal to 25% and the relative density of the dense layer is equal to 80%

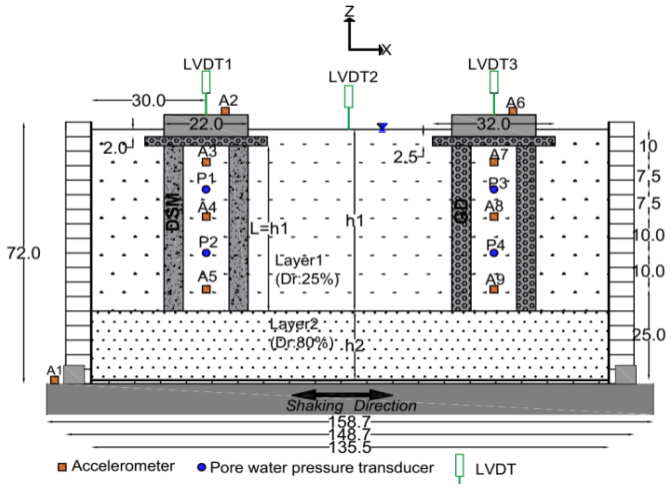

Fig. 7 Box section and model (dimensions in centimeters)

columns. This layer acts as a load transfer platform, and its main function is to transfer overheads on DSM and GD columns by reducing vertical loads on soft soils. This layer reduces the differential displacement between modified and unmodified soils. The columns are placed on a hard layer at the bottom.

8. Performed shaking table tests

In this study, 10 experiments (one non-improved land model and nine improved land models) were performed. The details of the experiment are shown in Table 3. In these experiments, the effect of liquefiable soil layer thickness on the performance of two improvement methods (GD and DSM columns) was investigated. The peak input acceleration for all tests was approximately 0.2 g and was applied at frequencies of 1, 2, and 3 Hz.

9. Test results

In the present study, a series of experiments was performed to investigate the effects of liquefiable layer thickness, frequency, column length, and an improvement method to control liquefaction. Due to the existence of two layers with different thicknesses and relative densities and the existence of initial static shear stress, the dynamic behavior of these sites was complex (Bertalot et al., 2013). In the following part, the parameters are discussed separately.

9.1 Acceleration

Acceleration can be an indicator of both detecting liquefaction initiation and the effectiveness of methods for dealing with it. After liquefaction occurs, the strength and stiffness of the soil decrease severely, so the shear waves get attenuated and the amplitude of accelerations at the ground is decreased. By utilizing improvement methods such as DSM and GD columns to counteract liquefaction, the values of damping and shear strains are reduced and the values of accelerations at the ground surface become higher than in the unimproved case. The time histories of the input base acceleration at frequencies of 1, 2, and 3 Hz are presented in Fig. 8. The loading of the system was harmonious, and the loading time in all the tests except Test A was eight seconds. The loading time of test A was 20

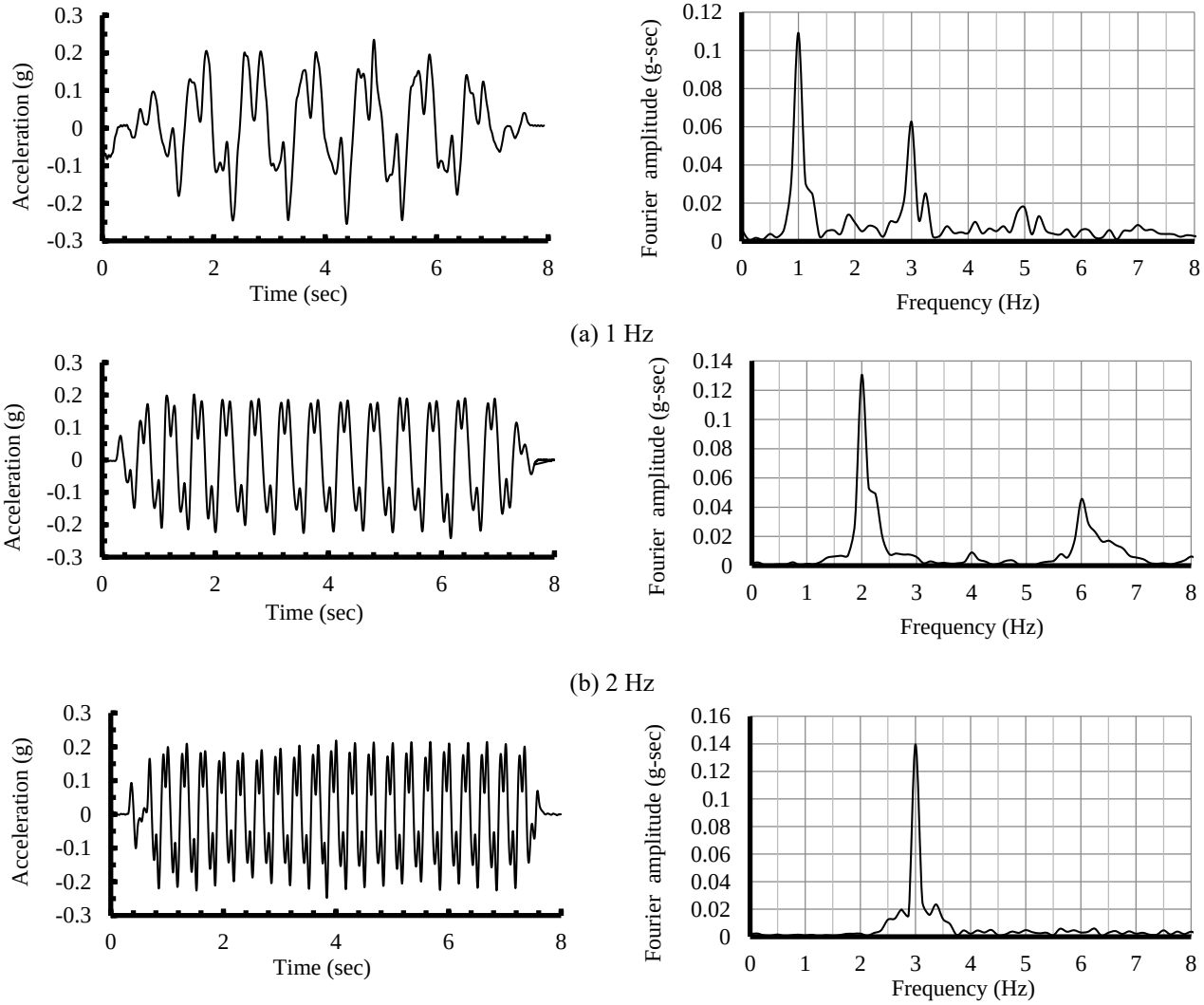

(a) 1 Hz

(b) 2 Hz

(c) 3 Hz

Fig. 8 Input acceleration time history and frequency content (a,b,c)

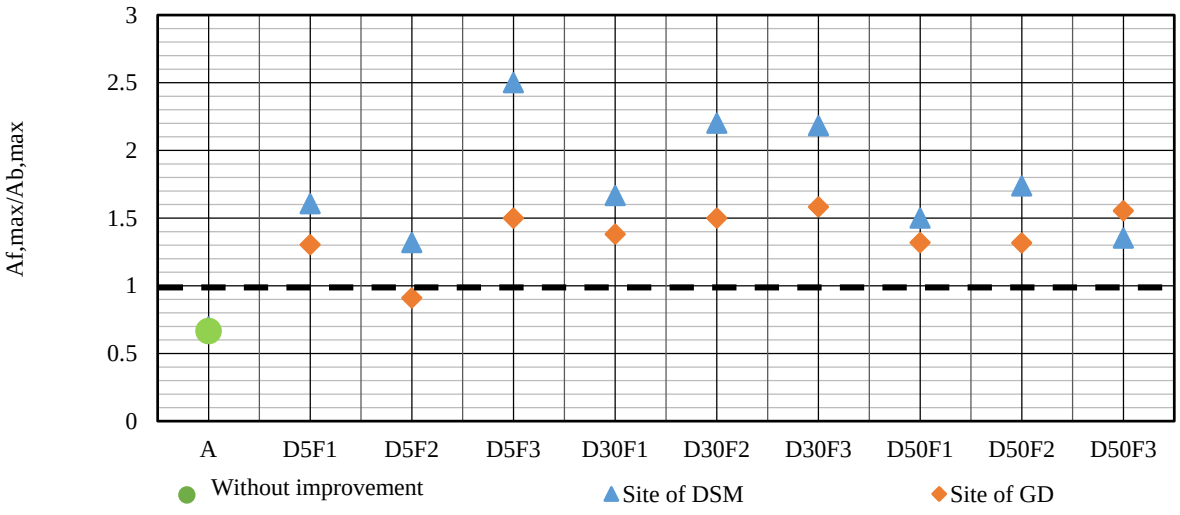

Fig. 9 Acceleration peak on the foundation at all tests

seconds. Because in the test A(untreated), liquefaction(ru=1) was occurred in two seconds, so this test was loaded in much longer time in order to investigate the liquefaction effects on foundation such as sinking, overturning and etc. The number of load cycles depending on the input load frequency for the frequencies of 1, 2, and 3 Hz was 8, 16, and 24 cycles, respectively. Baseline drift modification and band-pass filters between 0.01 and 20 Hz were conducted to eliminate noise in the high-frequency range and drift in the low-frequency range (Rayhani and El Naggar 2008).

The values of maximum accelerations on the foundation surface (A2, A6) in the improved and unimproved ground at different loads were considered to investigate the effects of liquefiable layer thickness on the dynamic responses of the foundation system and the improved soil. The results are presented in Fig. 9. In this diagram, the ratio of maximum acceleration at the foundation level (Af,max) to maximum base acceleration (Ab,max) in all the tests was calculated. In the improved ground in the D5 series tests (i.e., the thick liquefaction-prone layer), liquefaction occurred after a number of applied cycles. Despite the increase in acceleration amplitude in the first loading cycles, it finally decreased due to liquefaction of acceleration amplitudes.

According to Fig. 9, only in the unimproved site (Test A) was the ratio of maximum acceleration on the foundation to the maximum base acceleration ($A_{f,max}/A_{b,max}$) less than unity. The mentioned acceleration mitigation is due to liquefaction, a considerable decrease in soil stiffness, and increased damping. In contrast, this ratio is more than unity in the improved sites and is much higher in the modified ground with DSM columns than that with GD columns. In the unimproved case, structural damage due to inertial forces was much less than in the improved case. At D50F1 to D50F3 tests, the thickness of the liquefiable layer (h1) was the least, and the amount of ($A_{f,max}/A_{b,max}$) in both improvement techniques became much closer. At the 3-Hz input frequency, the ($A_{f,max}/A_{b,max}$) ratio in two different improvement methods was more dissimilar than at other frequencies.

9.2 Time history of the excess pore water pressure ratio

Excess pore water pressure is an important factor to consider when studying the seismic behavior of saturated loose sands. The excess pore water pressure ratio is defined as ($\boldsymbol{ru = \Delta u/\sigma_0'}$). In a loose saturated soil mass prone to liquefaction, if the soil layer is thick, the tendency to settle and produce excessive pore water pressure will be high. In this case, the degree of softening of the soil under the foundation will also be increased. Conversely, in loose saturated sandy soils, as the thickness of the layer is decreased, the amount of pore water pressure produced will be proportionally reduced. Further, the softening of the soil beneath the foundation and, consequently, its subsidence will be reduced. Meanwhile, the loading frequency can affect the pore water pressure response in any thickness.

The use of soil improvement methods such as DSM and GD columns can affect the amount of excess pore water pressures and, consequently, the percentage of soil softening under the foundation. Fig. 10 shows the diagram of the pore water pressure in Test A at a loading frequency of 2 Hz. Regarding Fig. 10, the value of ru at a depth of 35 cm (P_2) is greater than at a depth of 17.5 cm (P_1), meaning the amount of effective stress reduction at a depth of 35 cm will be greater than at a depth of 17.5 cm. This occurrence was the reverse of what was expected and is related to the effect of the presence of the foundation. Due to the presence of static shear stress, the soil showed a dilative behavior, and, therefore, the values of excess pore water pressure below the foundation were lower (the p1 and p3 transducers). Meanwhile, the cyclic liquefaction behavior changed to cyclic mobility beneath the foundation. Furthermore, the durability of the pore water pressures at the p1 transducer was greater than at the p2 transducer, which can be attributed to the formation of hydraulic gradients and the movement of pore water pressure produced from deeper levels to higher levels (Shown by dashed lines**)**. In other words, the excess pore pressure dissipation started from the deeper parts and then expanded to the shallower parts. This trend occurred during the 1995 Kobe earthquake, in which upward seepage was observed on Rokko Island until one hour after the earthquake. Such a transfer of water to the surface layers severely reduces soil resistance and creates secondary liquefaction and large deformations of the soil (Sadrekarimi and Ghalandarzadeh 2005). As it is clear from Fig. 10(a), complete liquefaction occurs approximately in the second loading cycle. The formation of vertical and horizontal hydraulic gradient causes a further increase of ru at p2 transducer and even exceed the excess pore pressure ratio of 1. This phenomenon has also been reported by Tsukamoto et al. (2012).

In the following, the excess pore water pressure ratio in Test A is compared with reinforced models (Fig. 10). For example, the results of Test D5F2, which has the liquefiable layer thicknesses similar to Test A, are presented. The amount of ru in the improved model has been decreased significantly. It is also observed that in the improved site with GD columns, the graph has a sharp peak compared to the improved site with DSM columns. The values of ru in place of DSM columns are lower than GD columns, and this shows that the DSM columns had better controlled the shear strains.

Another point was the time to reach the maximum value of ru in the models. As can be seen, at Test A, the time to reach full liquefaction (ru=1) is very short (almost in the second cycle), but at the improved models, the time to reach the maximum ru (ru<1) is much higher than the unimproved model and this time in DSM columns is much higher than GD columns. The results are shown at Fig. 10 as red dashed lines with arrows. Fig. 11 shows the parameter rumax at depths of 35 cm and 17.5 cm at the improved site with GD and DSM columns with different liquefiable layer thicknesses and loading frequencies. The thickness of the liquefiable layer and the frequency of the input motion have important effects on the maximum values of the ru. The rumax values in the unimproved ground (Test A) were higher than in other cases, and complete liquefaction occurred. However, in other tests, due to soil improvement under the foundation, soil behavior and responses changed significantly, and the value of the excess water pressure ratio was generally reduced. The rumax values reached a maximum value of 0.75 with the

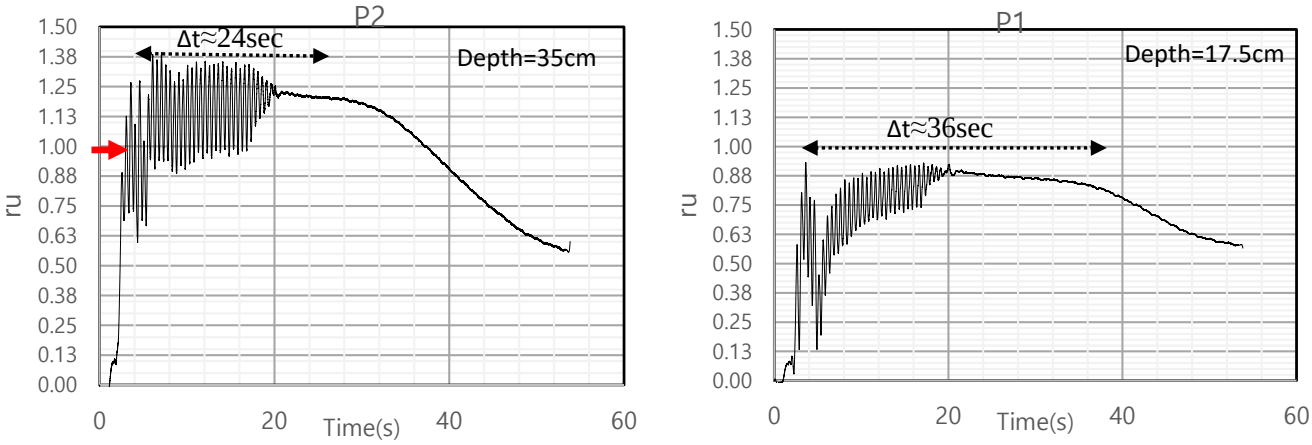

(a) Test A

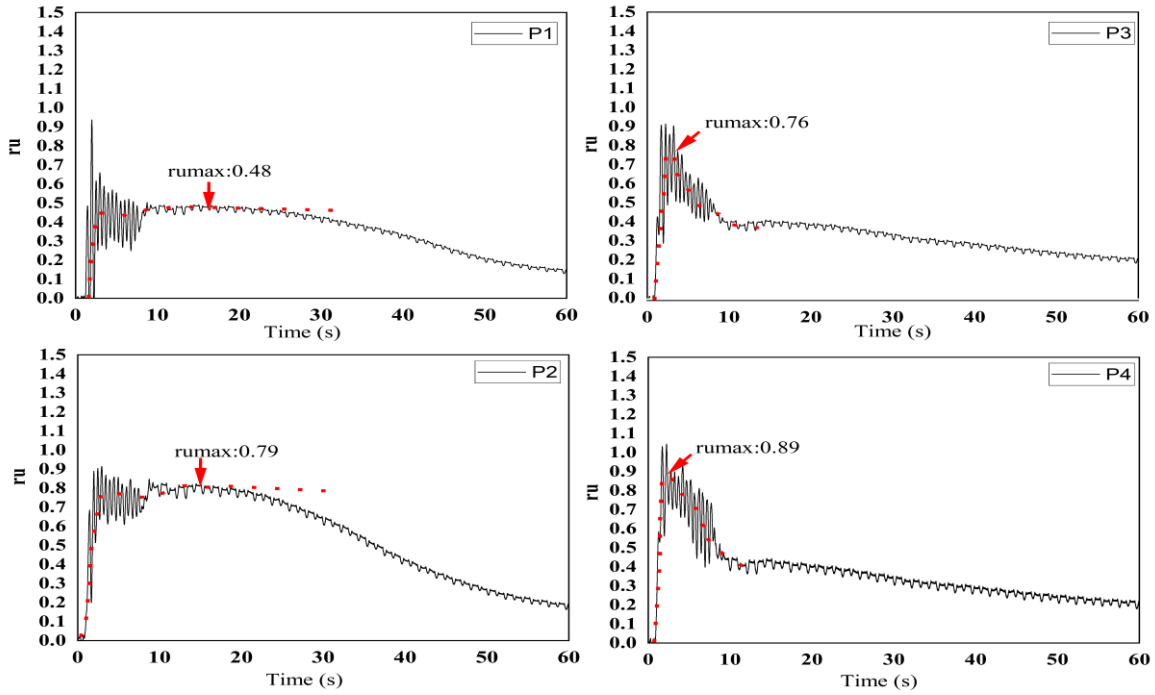

(b) Test D5F2

Fig. 10 Excess pore water pressure ratio (a,b)

application of soil improvement, which indicates a reduction of at least 40% of liquefaction potential. In general, the values of ru decreased significantly with decreasing the thickness of the liquefiable layer. In the surface layers (level of transducers P1, P3), rumax at different thicknesses of the liquefiable layer was affected by the frequency of the input motion. At 2 Hz, rumax deceased regularly as the thickness of the liquefiable layer decreased, but at other frequencies, this process was slightly irregular. In general, the rumax value is a very convenient parameter for explaining the interior circumstances of the complicated problem of liquefaction with different influencing factors.

9.3 Settlement

Foundation movement due to liquefaction originates from three different mechanisms: ejecta-induced, shear-induced, and volumetric-induced deformations (Bray and Dashti 2014). Ejection is ground loss beneath the foundation and was not observed in our experiments. Shear-induced settlement from punching failure or soil-structure-interaction ratcheting, which is a considerable part of the occurred settlement. The third mechanism is volumetric-induced settlement from sedimentation or post-liquefaction consolidation. Consolidation occurs due to the disappearance of excess pore water pressure. The response and participation of each of these settling mechanisms in the general displacement of the structure is a function of soil and structural properties and ground motion characteristics. In the liquefiable soil case, the phenomenon of settlement could also be considered subsidence because of its abrupt occurrence.

Bahmanpour *et al.* (2019) showed that foundation subsidence is a key parameter in determining the

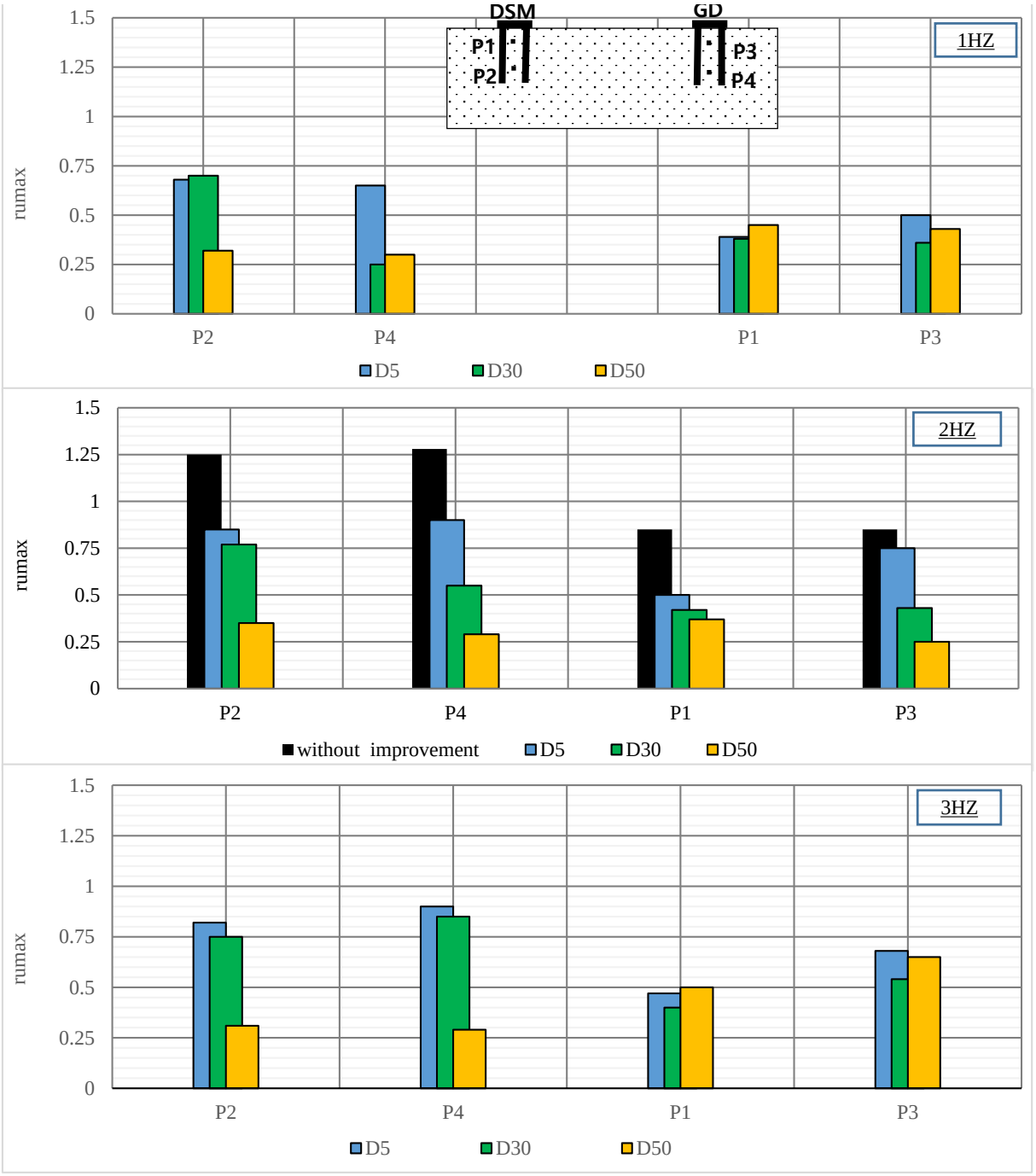

Fig. 11 Distribution of maximum ru values in different thickness and loading frequency

effectiveness of soil reinforcement columns. Soil failure under a foundation is the result of a decrease in soil strength due to an increase in the pore water pressure and a sharp decrease in effective stresses. In the unimproved ground (Test A), after the dynamic load was applied at the second loading cycle, the foundations were completely sunk into the ground and penetrated 65 cm deep into the soil. The reason for this catastrophic event is the considerable depth of the liquefied layer and the loss of stiffness and shear strength of the soil due to the generation of excess pore water pressure in the loose soil mass under the foundation.

In other models, the value of settlements was drastically reduced by soil reinforcement. The results of the settlement of foundations and free field are presented in Fig. 12 for all tests. As it is depicted, with the reduction of liquefiable layer thickness, the maximum values of settlements decrease considerably. In general, the maximum settling values in the foundation located on GD columns (LVDT3) were higher than the foundation settlement of DSM columns (LVDT1). This settling difference was much more pronounced in models with thicker liquefiable layers. Free-field settlement (LVDT2), which is attributed to volumetric settlement, ranged from 4 to 15 mm, which is much less than foundation settlements. One important parameter

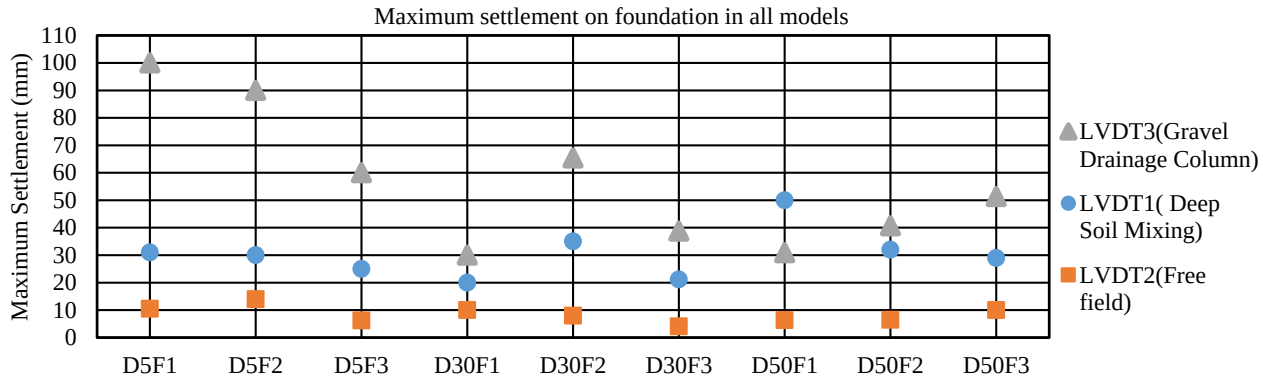

Fig. 12 Maximum settlement of foundations and free field area

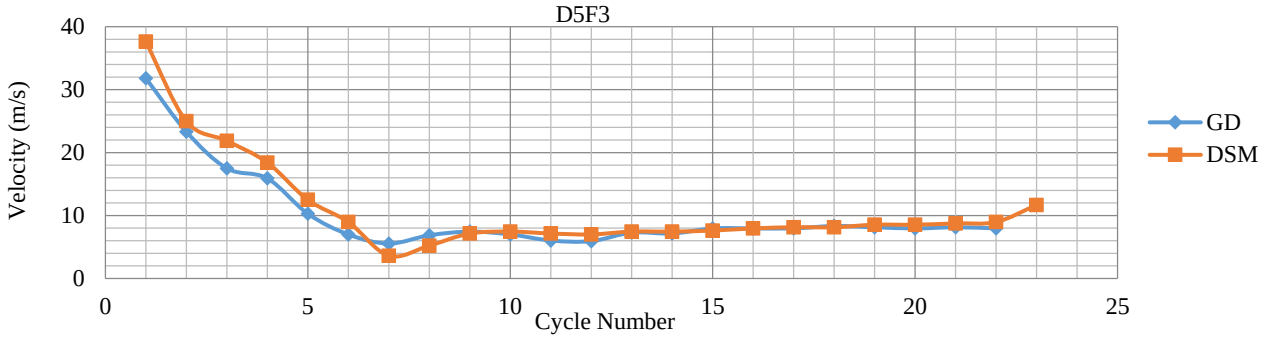

Fig. 13 Improved ground shear wave velocity versus load cycles in D5F3 test

affecting the performance of long load-bearing elements such as DSM columns is the confining stress, which has a direct effect on the flexural and axial strength and effectiveness of columns. The effect of confining pressure on columns with low axial stiffness, such as GD columns, is very decisive. Due to the conditions of the experiment (saturated loose subsurface layers), the values of confining stresses were very low. Thus, when the GD column was built on very soft ground, there was not enough lateral limitation of the surrounding soil. Therefore, in GD columns that have less stiffness than DSM columns, lower lateral stresses led to the formation of bulging failure at shallow depths of 1.5 ~ 3 times the diameter of the column (Castro 2017) and caused more subsidence and severe reductions in effectiveness. Therefore, GD columns are not proposed in thick liquefiable stratum.

In the case of DSM columns, as the depth of the burial of the column increases, its resistance value becomes more active. This is why, despite the high thickness of the liquefiable layer (D5 class tests), the values of foundation settlement on DSM columns were less than on GD columns. However, the stiffness of DSM columns affects their performance in reducing settlements in liquefiable soil. According to the maximum foundation settlements diagram, when the thickness of the liquefiable layer decreased (D50 series tests), the settlement in the foundation located on the GD columns also decreased. According to Fig. 11, it can be seen that in the reinforced models, the excess pore water pressure ratio reached less than 0.75, so in these models, the complete liquefaction phenomenon did not occur, and the settlements are caused by pore pressure buildup and the cyclic softening of the underlying sand layers.

Based on the settlement measurements, it can be concluded that thin liquefiable layers result in similar foundation settlements located on both GD and DSM columns. Due to the fact that the implementation of DSM columns requires special equipment and labor and costs more than GD columns, in cases where the thickness of the liquefiable layer is low, GD columns can be preferred. Important structures can utilize the combined method of GD and DSM columns for much more precise control of settlements.

9.3.1 Impact of frequency on subsidence

The variation of shear wave velocity during shaking at the center of a loose liquefiable layer of test series D5 is presented in Fig. 13. The calculation was implemented based on the time lag between two acceleration transducers.

The Acceleration transducers used in the models have high data recording accuracy and their sampling rate is 1000 sample per second. As depicted, the shear wave velocity decreased from 36 m/s to 4 m/s which is due to pore pressure buildup and the softening of the underlying sand layers. Also, by utilizing Eq. (6), the characteristic period (Ts) corresponding to the fundamental frequency can be calculated (Kramer 1996).

$$T_S = \frac{4h}{v_s} \quad (6)$$

Where, h is the thickness of the loose soil layer, and vs is the shear wave velocity.

Of course, assuming the shear strain compatibility, the calculated velocity was equal to the average shear wave velocity equivalent to the improved ground. Therefore, the

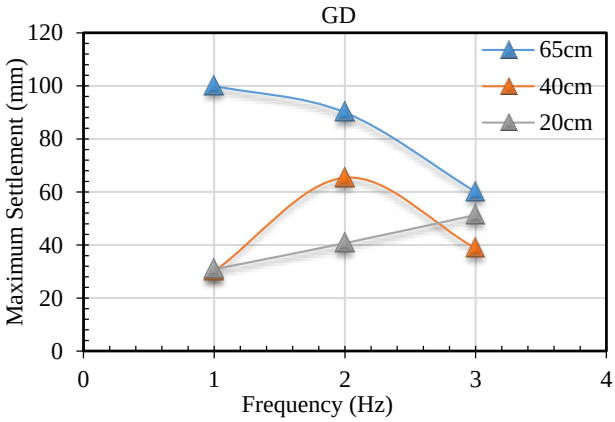

Fig. 14 Distribution of maximum settlement at different frequencies in the improved site with GD

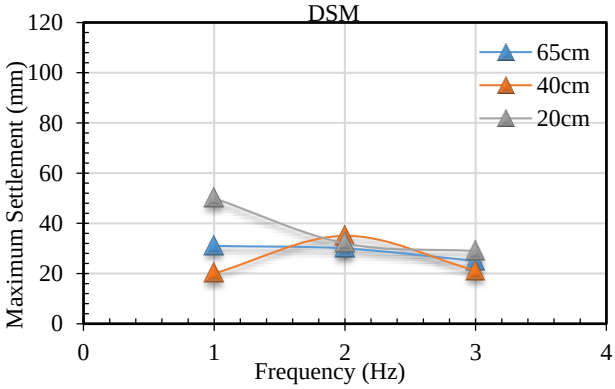

Fig. 15 Distribution of maximum settlement at different frequencies in the improved site with DSM

dominant frequencies in the D5 test series at the beginning and end of the test were estimated to be 14 Hz and 1.45 Hz, respectively. In other words, the dominant frequency of the system is decreased due to pore water pressure buildup. The amount of input frequency in the soil system and foundation at different thicknesses in liquefiable soil has diverse effects on the subsidence behavior of the foundation. As can be seen from Fig. 14, the maximum settlement values at different thicknesses of the liquefiable soil layer are related to its input frequency. In GD columns in the D5 test series, where the thickness of the liquefaction layer was high, the maximum settlement value was much higher at 1 Hz compared with higher frequencies. Also, in the D30 series tests, where the thickness of the liquefiable layer was 40 cm, the amount of subsidence at 2 Hz was higher than at other frequencies. In the D50 series tests, where the thickness of the liquefiable layer was low, the subsidence at a frequency of about 3 Hz was more than at other frequencies. This general trend could be attributed to the reality that in thick liquifiable layer the dominant frequency is lower and so in low input frequencies the resonance phenomenon causes larger settlements.

According to Fig. 15, which is related to DSM, it seems that the changes in settlement at different thicknesses based on the frequency of input movement to the model are very small. Therefore, in the improved site with DSM columns, the effect of input motion frequency on the maximum settlement of the foundation is not very obvious, especially

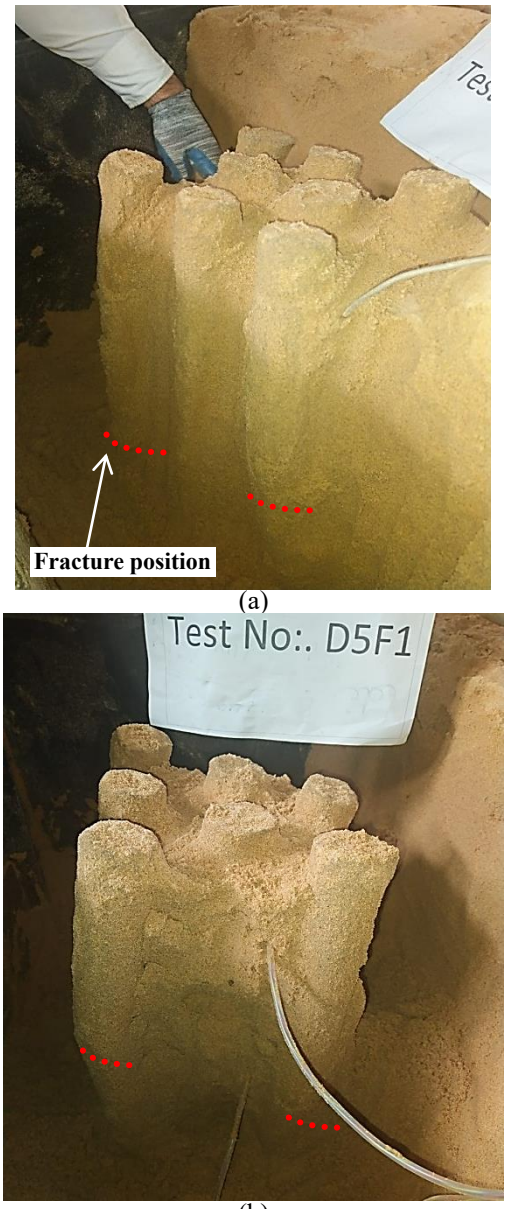

(a)

(b)

Fig. 16 Fracture of DSM columns at D5F1 test (a,b)

at higher frequencies. The lower influence of input frequency on the settlement values in DSM columns as compared with GD columns can be attributed to the larger stiffness of the DSM columns.

9.4 Failure mechanism

In DSM columns that were applied in a layer with a high liquefiable thickness (D5 series), fractures were observed as shown in Fig. 16. This fracture was not observed in DSM columns in D30 and D50 series tests. This indicates that if the DSM columns have more burial depth, the columns will bend and cut, and this will cause the columns to break in the thick liquefiable layers. On the other hand, Fig. 17 illustrates the bulging of the GD columns. Due to the looseness of the layer and the lack of confining stresses of the columns of this model, failure in GD columns occurred.

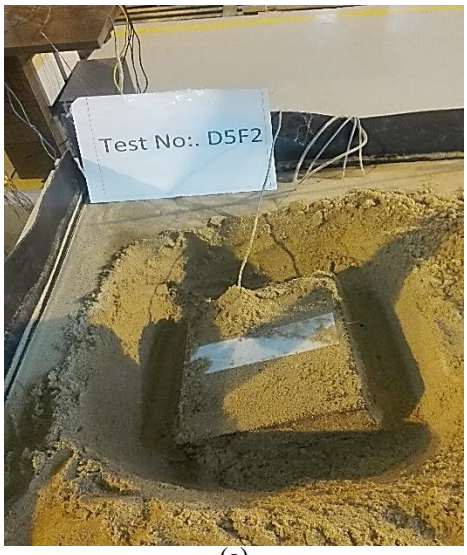

(a)

(b)

Fig. 17 bulging and foundation settlement on the GD columns (a,b)

9.5 Rate of settlement

Another important parameter that can directly affect the percentage of damage to structures and vital lifelines is the rate of subsidence. Due to the importance of servicing vital buildings after an earthquake and the stability of service, this issue is crucial. The rate of subsidence of the foundation located on the loose liquefiable layer depends on many variables, including the foundation overhead stress, liquefiable layer thickness, relative density of subsurface layers, frequency content, and the type and arrangement of soil improvement elements. To calculate the rate of settlement of the foundation placed in the reinforced ground in each of the tests, the slope of the time settlement graph in the loading phase has been calculated. Fig. 18 shows the distribution of settlement rate at the foundations and the free field in different tests. As can be seen, the rate of settlement of the foundation increased when the thickness of the saturated loose layer was high. Decreasing the thickness of the liquefiable layer reduced the rate of settlement. The rate of settlement in the free field was very low due to the lack of static shear stress. DSM columns worked very well in controlling the rate of settlement. According to the interpretations made for the maximum settlement at different frequencies, the same events were reflected here. It was observed that in the liquefiable layer with great depth (D5 test series), the amount of the settlement rate at 1Hz was higher than at other frequencies. In the D50 test series, the amount of settlement rate at 3 Hz was higher than at other frequencies. Therefore, the thickness of the liquefiable layer and the frequency of input motion can significantly affect the response to subsidence.

9.6 Rotation of the foundation

In order to calculate the rotation of the foundation, after the completion of the test, the settlement at the corners of the rigid foundation was measured by a caliper and based on the trigonometric relations, the amount of rotation of the foundations was calculated. Fig. 19 shows the rotation of the foundation in units of degree in two improved sites. As can be seen in the non-improved site (Test A), the rotation of the foundation was very high. In this model, the foundation was completely immersed in the subsurface layer. In other tests, the amount of foundation rotation was reduced. In the improved site with a high liquefaction layer thickness (D5 test series) at a frequency of 1 Hz, the foundation rotation was higher than at other frequencies. In the D30 series test, the amount of foundation rotation at 2 Hz was higher than at other frequencies. In the model with the thin liquefaction layer (the D50 series), the amount of rotation decreased as the frequency increased. As can be observed from diagram 19, in general, with the decrease in the thickness of the liquefaction-prone layer, the rotation of the foundation has also decreased significantly. Therefore, the thickness of the liquefaction layer and the input frequency have a significant effect on the rotational response of the foundation

10. Conclusions

The main purpose of this paper is to investigate the effect of liquefiable layer thickness on the dynamic behavior of the foundation placed on a saturated loose sand layer that has been improved by two techniques of deep mixing columns (DSM) and gravel drain columns (GD). Ten tests were carried out, one of which was unmodified and nine of which were modified with columns. The main results of the experiments are as follows:

(a) Acceleration peak and input frequency affect the acceleration response at ground level. The ratio of the input acceleration peak to the horizontal acceleration peak at the foundation level in the non-improved model (Test A) was less than unity, while in the improved ground, this ratio was more than unity.

(b) Deep mixing columns have significantly magnified ground surface accelerations compared with gravel drain columns, indicating that the ground is reinforced with deep mixing columns.

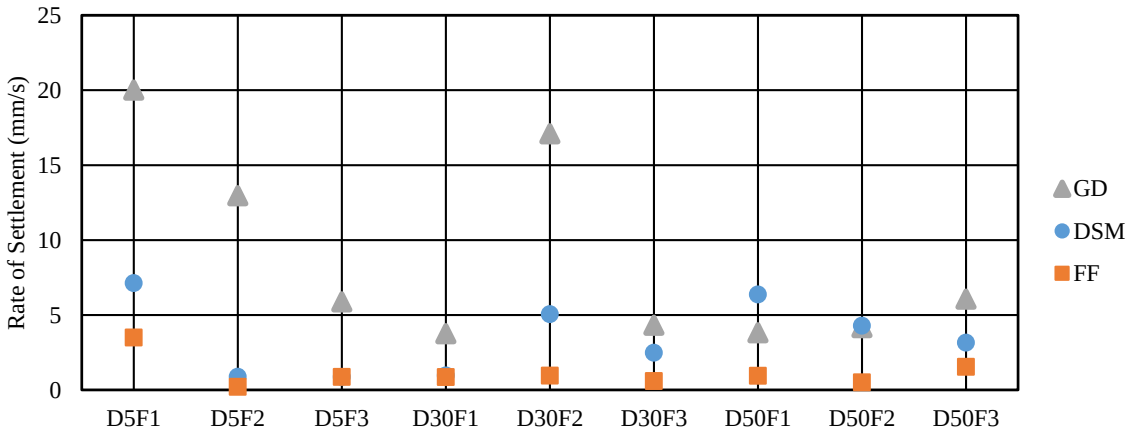

Fig. 18 Settlement rate at improved foundations and free field

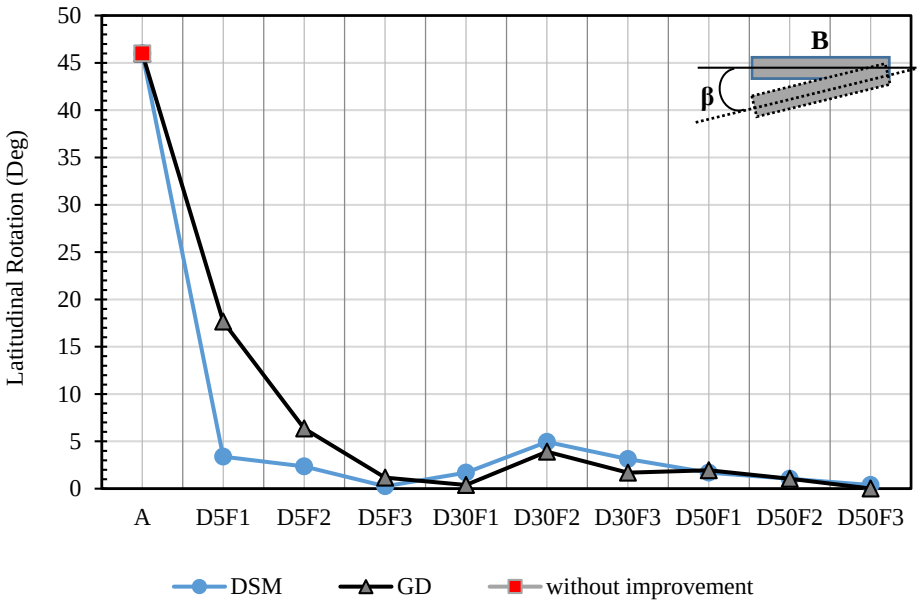

Fig. 19 Rotation of the foundation at all tests

(c) In the thick liquefaction layer (Test A), the values of the excess pore water pressure ratio (Ru) are high, and their durability is much longer than in the rest of the tests. Thus, the time of redistribution of effective stresses and reaching a stable value is longer than in other tests.

(d) In gravel drain columns, bulging, which is caused by the lack of confining stresses, causes large subsidence in the foundation. Meanwhile, in deep mixing columns, due to high stiffness compared to gravel columns and reduced excess pore water pressure, the value and rate of settlements decrease.

(e) The range of maximum settlements in the foundation depends on the frequency of the input movement and the thickness of the loose sand layer. At higher thicknesses (D5 series tests), the maximum settlement values are highest at the 1-Hz input frequency. If the thickness of the saturated loose layer decreases, the settlement values at the higher input frequencies increases.

(f) As the thickness of the saturated loose layer decreases, the effect and dynamic behavior of the gravel columns become closer to the deep mixing columns. Therefore, in variable thickness layers, time and cost can be saved by choosing the optimal improvement method.

(g) Due to the frequency changes in liquefiable soil, the designer must model the entire system to identify the forces acting correctly on the foundation to obtain the system response.

(h) In the unimproved site (Test A), nearly all the foundation settlements occurred at the beginning of shaking. On the contrary, most of the settlements in reinforced models are caused by the accumulation of excess pore water pressures and soil softening during the whole loading time history.

(i) The thickness of the liquefiable layer is a key parameter in determining the best improvement technique that can directly affect the dynamic performance of the foundation and structure.

References

Araei, A.A. and Towhata, I. (2014), "Impact and cyclic shaking on loose sand properties in laminar box using gap sensors", *Soil Dyn. Earthq. Eng*., **66**, 401-414. https://doi.org/10.1016/j.soildyn.2014.08.004.

Asgari, A., Oliaei, M. and Bagheri, M. (2013), "Numerical simulation of improvement of a liquefiable soil layer using stone column and pile-pinning techniques", *Soil Dyn. Earthq. Eng*., **51**, 77-96. https://doi.org/10.1016/j.soildyn.2013.04.006.

Bahadori, H., Ghalandarzadeh, A. and Towhata, I. (2008), "Effect of non plastic silt on the anisotropic behavior of sand", *Soils Found*., **48**(4), 531-545. https://doi.org/10.3208/sandf.48.531.

Bahmanpour, A., Towhata, I., Sakr, M., Mahmoud, M., Yamamoto, Y. and Yamada, S. (2019), "The effect of underground columns on the mitigation of liquefaction in shaking table model experiments", *Soil Dyn. Earthq. Eng*., **116**, 15-30. https://doi.org/10.1016/j.soildyn.2018.09.022.

Bayati, H. and Bagheripour, M.H. (2019), "Shaking table study on liquefaction behaviour of different saturated sands reinforced by stone columns", *Mar. Georesour. Geotec*., **37**(7), 801-815. https://doi.org/10.1080/1064119X.2018.1492051.

Bertalot, D., Brennan, A. and Villalobos, F. (2013), "Influence of bearing pressure on liquefaction-induced settlement of shallow foundations", *Géotechnique*, **63**(5), 391. https://doi.org/10.1680/geot.11.P.040.

Bouassida, M. and Porbaha, A. (2004), "Ultimate bearing capacity of soft clays reinforced by a group of columns: Application to a deep mixing technique", *Soils Found*., **44**(3), 91-101. https://doi.org/10.3208/sandf.44.3_91.

Bray, J.D. and Dashti, S. (2014), "Liquefaction-Induced Building Movements", *Bull. Earthq. Eng*., **12**(3), 1129-1156. https://doi.org/10.1007/s10518-014-9619-8.

Brown, R.E. (1977), "Vibroflotation compaction of cohesionless soils", *J. Geotech. Eng. Division*., **103**(12), 1437-1451. https://doi.org/10.1061/AJGEB6.0000538.

Brennan, AJ. and Madabhushi, S.P.G. (2002), "Effectiveness of Vertical Drains in Mitigation of Liquefaction", *Soil Dyn. Earthq. Eng.*., **22**(9-12), 1059-1065. https://doi.org/10.1016/S0267-7261(02)00131-8.

Castro, J. (2017), "Groups of encased stone columns: Influence of column length and arrangement", *Geotext. Geomembranes*, **45**(2), 68-80. https://doi.org/10.1016/j.geotexmem.2016.12.001.

DehqanKhalili, H., Ghalandarzadeh, A., Moradi, M. and Karimzadeh, R. (2020), "Effect of distribution patterns of DSM columns on the efficiency of liquefaction mitigation", *Scientia Iranica*., **27**(5), 2198-2208. https://doi.org/10.24200/sci.2019.21647.

Esmaeili, M., Gharouni-Nik, M. and Khajehei, H. (2014), "Evaluation of deep soil mixing efficiency in stabilizing loose sandy soils using laboratory tests", *Geotech. Test. J*., **37**(5), 817-827. https://doi.org/10.1520/GTJ20130099.

Farahmand, K., Lashkari, A. and Ghalandarzadeh, A. (2016), "Firoozkuh sand: introduction of a benchmark for geomechanical studies", *Iranian J. Sci. Technol. T. Civil Eng*., **40**(2), 133-148. https://doi.org/10.1007/s40996-016-0009-0.

Fattah, M.Y., Al-Neami, M.A. and Al-Suhaily, A.S. (2017), "Estimation of bearing capacity of floating group of stone columns", *Eng. Sci. Technol. Int. J*., **20**(3), 1166-1172. https://doi.org/10.1016/j.jestch.2017.03.005.

Green, R.A., Olgun, C.G. and Wissmann, K.J. (2008), "Shear stress redistribution as a mechanism to mitigate the risk of liquefaction", *In Geotech. Earthq. Eng. Soil Dyn.*., IV, 1-10. https://doi.org/10.1061/40975(318)115.

Hasheminezhad, A. and Bahadori, H. (2019), "Seismic response of shallow foundations over liquefiable soils improved by deep soil mixing columns", *Comput. Geotech*., **110**, 251-273. https://doi.org/10.1016/j.compgeo.2019.02.019.

Hasheminezhad, A. and Bahadori, H. (2020), "On the deep soil mixing method in the mitigation of liquefaction-induced bearing capacity degradation of shallow foundations", *Geomech. Geoeng*., 1-13. https://doi.org/10.1080/17486025.2020.1755460.

Iai, S. and Koizumi, K. (1986), "Estimation of earthquake induced excess pore water pressure for gravel drains", *Proceedings of the 7th Japan Earthquake Engineering Symposium*., 679-684. https://doi.org/10.2208/jscej.1996.535_155.

Iai, S. (1989), "Similitude for shaking table tests on soil-structure-fluid model in 1g gravitational field", *Soils Found*., **29**(1), 105-118. https://doi.org/10.3208/sandf1972.29.105

Kayabasi, A. and Gokceoglu, C. (2018), "Liquefaction potential assessment of a region using different techniques (Tepebasi, Eskişehir, Turkey)", *Eng. Geol*., **246**, 139-161. https://doi.org/10.1016/j.enggeo.2018.09.029.

Kitazume, M. (1996), "JGS TC Report: Japanese design procedures and recent activities of DMM", 925-937.

Kitazume, M., Yamazaki, H. and Tsuchida, T. (2000), "Recent soil admixture stabilization techniques for port and harbor constructions in Japan—deep mixing method, premix method, light-weight method", 23-40.

Kramer, S.L. (1996), *Geotechnical earthquake engineering* (Pearson Education India).

Lee, C.J., Wei, Y.C. and Kuo, Y.C. (2012), "Boundary effects of a laminar container in centrifuge shaking table tests", *Soil Dyn. Earthq. Eng*., **34**(1), 37-51. https://doi.org/10.1016/j.soildyn.2011.10.011.

Liu, L. and Dobry, R. (1997), "Seismic response of shallow foundation on liquefiable sand", *J. Geotech. Geoenviron. Eng.*, **123**(6), 557-567. https://doi.org/10.1061/(ASCE)1090-0241(1997)123:6(557).

Lou, M., Wang, H., Chen, X. and Zhai, Y. (2011), "Structure–soil–structure interaction: Literature review", *Soil Dyn. Earthq. Eng*., **31**(12), 1724-1731. https://doi.org/10.1016/j.soildyn.2011.07.008.

Miyajima, M., Setiawan, H., Serikawa, Y. and Yoshida, M. (2019), "Liquefaction-induced damage in recent earthquakes and new countermeasures against liquefaction", *In IACGE 2018: Geotechnical and Seismic Research and Practices for Sustainability*., 557-565, American Society of Civil Engineers Reston, VA.

Namikawa, T., Koseki, J. and Suzuki, Y. (2007), "Finite element analysis of lattice-shaped ground improvement by cement-mixing for liquefaction mitigation", *Soils Found*., **47**(3), 559-576. https://doi.org/10.3208/sandf.47.559.

Orense, R., Morimoto, I., Yamamoto, Y.A., Yumiyama, T., Yamamoto, H. and Sugawara, K. (2003), "Study on wall-type gravel drains as liquefaction countermeasure for underground structures", *Soil Dyn. Earthq. Eng*., **23**(1), 19-39. https://doi.org/10.1016/S0267-7261(02)00152-5.

Ozden, S., Akpinar, E., Erdogan, H. and Atalay, HM. (2014), "Performance of precast concrete structures in October 2011 Van earthquake, Turkey", *Mag. Concrete Res*., **66**(11), 543-552. https://doi.org/10.1680/macr.13.00097.

Porbaha, A., Zen, K. and Kobayashi, M. (1999), "Deep mixing technology for liquefaction mitigation", *J. Infrastruct. Syst*., **5**(1), 21-34. https://doi.org/10.1061/(ASCE)1076-0342(1999)5:1(21).

Prasad, S., Towhata, I., Chandradhara, G. and Nanjundaswamy, P. (2004), "Shaking table tests in earthquake geotechnical engineering", *Current Sci*., **87**(10), 1398-1404. https://www.jstor.org/stable/24109480.

Rayamajhi, D., Nguyen, T.V., Ashford, S.A., Boulanger, R.W., Lu, J., Elgamal, A. and Shao, L. (2014), "Numerical study of shear stress distribution for discrete columns in liquefiable soils", *J.*

Geotech. Geoenviron. Eng., **140**(3), 04013034. https://doi.org/10.1061/(ASCE)GT.1943-5606.0000970.

Rayhani, M.H. and El Naggar, M.H. (2008), "Seismic response of sands in centrifuge tests", *Can. Geotech. J*., **45**(4), 470-483. https://doi.org/10.1139/T07-097.

Sadrekarimi, A. and Ghalandarzadeh, A. (2005), "Evaluation of gravel drains and compacted sand piles in mitigating liquefaction", *Proceedings of the Institution of Civil Engineers-Ground Improvement*., **9**(3), 91-104. https://doi.org/10.1680/grim.2005.9.3.91.

Seed, H.B. and Booker, J.R. (1977), "Stabilization of potentially liquefiable sand deposits using gravel drains", *J. Geotech. Eng. Division*., **103**(7), 757-768. https://doi.org/10.1061/AJGEB6.0000453.

Shahraki, M., Rafiee-Dehkharghani, R. and Behnia, K. (2018), "Three-dimensional Finite Element modeling of stone column-improved soft saturated ground", *Civil Eng. Infrastruct. J*., **51**(2), 389-403. https://doi.org/10.7508/ceij.2018.02.009.

Siddharthan, R.V. and Porbaha, A. (2008a), "Seismic response evaluation of sites improved by deep mixing, Part 2: Verification", *Proceedings of the Institution of Civil Engineers-Ground Improvement*., **161**(3), 163-169. https://doi.org/10.1680/grim.2008.161.3.153.

Siddharthan, R.V. and Porbaha, A. (2008b), "Seismic response evaluation of sites improved by deep mixing, Part I: Proposed approach", *Proceedings of the Institution of Civil Engineers-Ground Improvement*., **161**(3), 153-162. https://doi.org/10.1680/grim.2008.161.3.163.

Tang, L., Cong, S., Ling, X., Lu, J. and Elgamal, A. (2015), "Numerical study on ground improvement for liquefaction mitigation using stone columns encased with geosynthetics", *Geotext. Geomembranes*, **43**(2), 190-195. https://doi.org/10.1016/j.geotexmem.2014.11.011.

Tsukamoto, Y., Ishihara, K., Sawada, S. and Fujiwara, S. (2012), "Settlement of rigid circular foundations during seismic shaking in shaking table tests", *Int. J. Geomech*., **12**(4), 462-470. https://doi.org/10.1061/(ASCE)GM.1943-5622.0000153.

Turan, A., Hinchberger, S.D. and El Naggar, H. (2009), "Design and commissioning of a laminar soil container for use on small shaking tables", *Soil Dyn. Earthq. Eng*., **29**(2), 404-414. https://doi.org/10.1016/j.soildyn.2008.04.003.

Yang, F.O., Fan, G., Wang, K., Yang, C., Lyu, W. and Zhang, J. (2021), "A large-scale shaking table model test for acceleration and deformation response of geosynthetic encased stone column composite ground", *Geotext. Geomembranes*, https://doi.org/10.1016/j.geotexmem.2021.05.013.

Zeng, X. and Schofield, A.N. (1996), "Design and performance of an equivalent-shear-beam container for earthquake centrifuge modelling", *Geotechnique*., **46**(1), 83-102. https://doi.org/10.1680/geot.1996.46.1.83.

Zhou, H.Z., Zheng, G., Yu, X.X., Zhang, T.Q. and Liu, J.J. (2018), "Bearing capacity and failure mechanism of ground improved by deep mixed columns", *J. Zhejiang Univ.-SCi. A*, **19**(4), 266-276. https://doi.org/10.1631/jzus.A1700517.